Electronic Supplementary Information (ESI) for

Hierarchical Two-Dimensional Molecular Assembly through Dynamic Combination of Conformational States at the Liquid/Solid Interface

Matsuhiro Maeda,[†] Ruri Nakayama,[†] Steven De Feyter[‡] Yoshito Tobe,[,¶,#] Kazukuni Tahara[*,†]*

[†]Department of Applied Chemistry, School of Science and Technology, Meiji University, 1-1-1 Higashimita, Tama-ku, Kawasaki, Kanagawa, 214-8571, Japan.

[‡]Division of Molecular Imaging and Photonics, Department of Chemistry, KU Leuven, Celestijnenlaan 200 F, 3001 Leuven, Belgium.

[¶]The Institute of Scientific and Industrial Research, Osaka University, Ibaraki, Osaka 567-0047, Japan. #Department of Applied Chemistry, National Chiao Tung University, 1001 Ta Hsueh Road, Hsinchu 30030, Taiwan.

correspondence to: tahara@meiji.ac.jp

This file includes:

1. Hypothetical SAMNs Formed by DBA-OC14-OH

Hydrogen bonding interactions have been widely used for designing self-assembled molecular networks (SAMNs) because of their strength and directionality. Moreover, there exist many examples of SAMNs formation using both hydrogen bonding (HB) interactions and van der Waals interactions as driving forces.[1–3] In the present study, we planned to construct hierarchical SAMNs at the liquid/graphite interfaces using **DBA-OC14-OH** as a molecular building block based on the following considerations. We hypothesize that (i) **DBA-OC14-OH** adopts geometries with different numbers (m = 0, 1, 2 or 3) of alkyl chains adsorbed by physisorption on the surface (*i.e.*, 3 – m = alkyl chains orienting to the solution phase) based on our previous study,[4] (ii) it assembles to form triangular clusters though intermolecular HB interactions between the hydroxy groups thanks to its C_3-symmetric shape, (iii) by adjusting the polarity of solvent, the size of the cluster changes depending on both absolute and relative numbers of different types of DBA of m = 0–2, and (iv) the clusters are connected by van der Waals interaction, forming honeycomb patterns (Fig. S1).[5,6]

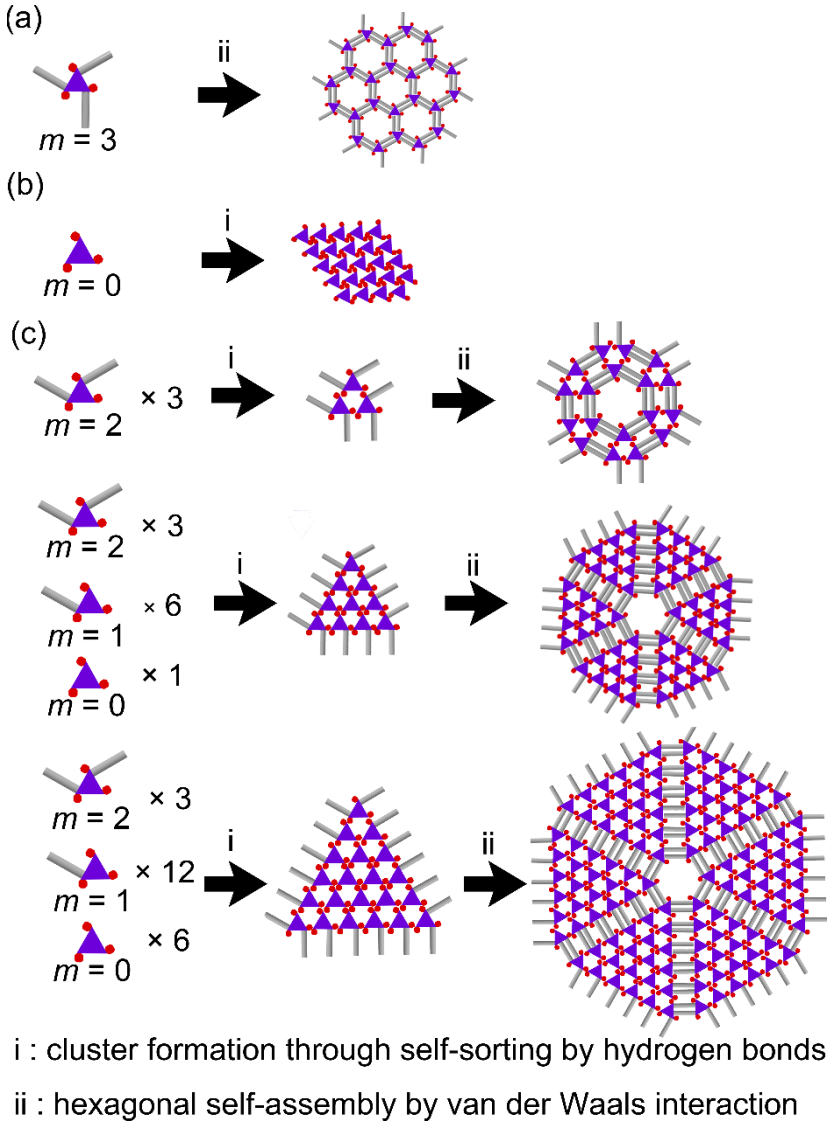

Fig. S1. Illustrations of conceived self-assembled structures formed by **DBA-OC14-OH**. Color code: purple; triangular π-core, grey; tetradecyloxy (OC14) group, red; hydroxy group. (a) A honeycomb structure formed by only van der Waals interactions. (b) A dense-packed structure formed by only hydrogen bonding interactions. (c) Hierarchical structures formed by both van der Waals and hydrogen bonding interactions. The tetradecyloxy groups orienting to a solution phase are omitted from this illustration. The HA molecules connecting the DBA molecules at the rim of hydrogen bonded clusters are omitted for clarity.

2. Self-Assembly of DBA-OC14-OH at the TCB/Graphite Interface

2-1. Additional STM Images

At the TCB/graphite interface, **DBA-OC14-OH** forms extended domains (larger than the image size of 80 × 80 nm^2) of the hexagonal porous structure independent of the solute concentration (Fig. S2).

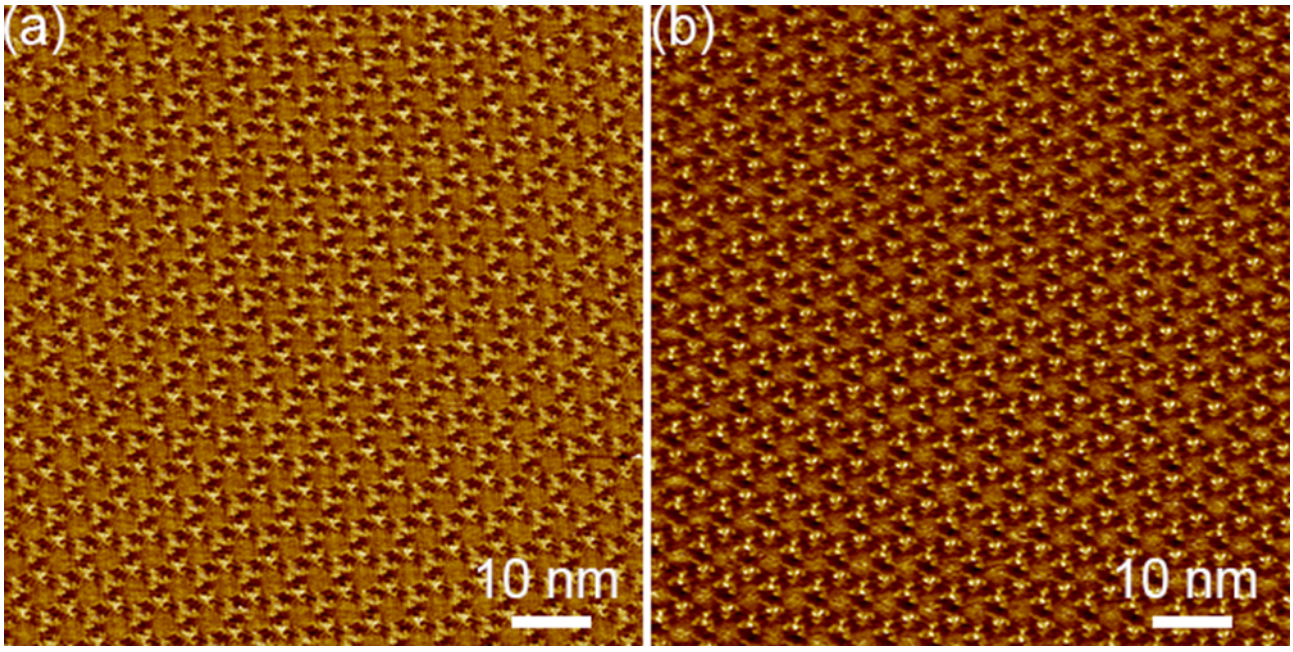

Fig. S2. STM images of a hexagonal porous structure (a) at 3.0×10^{-6} M (I_{set} = 100 pA, V_{bias} = –0.32 V) and (b) at 1.0×10^{-4} M (I_{set} = 300 pA, V_{bias} = –0.40 V).

2-2. Cross-Section Height Analysis for Interdigitated Alkyl Chains

In order to determine the number of the adsorbed alkyl chains located between adjacent triangle clusters, cross section height analyses were conducted. The heights of 10 cross sections were measured from four calibrated STM images (30 × 30 nm^2 or smaller). For instance, a line profile for cross section height analysis along the blue line in Fig. S3a is shown in Fig. S3b. In Fig. S3b, there

are seven peaks (pointed by red arrows) from edge to edge in the adsorbed alkyl chains. The average distance between the peaks was 0.46 ± 0.06 nm. This value is consistent with the optimal distance for van der Waals interaction between adjacent alkyl chains on graphite surface.[7,8] The seven peaks correspond to seven alkyl chains adsorbed between the adjacent clusters. The heights of the pore parts are typically higher than the alkyl chain parts. This could be attributed to mobile co-adsorbed TCB molecules, that show higher conductivity.[9,10]

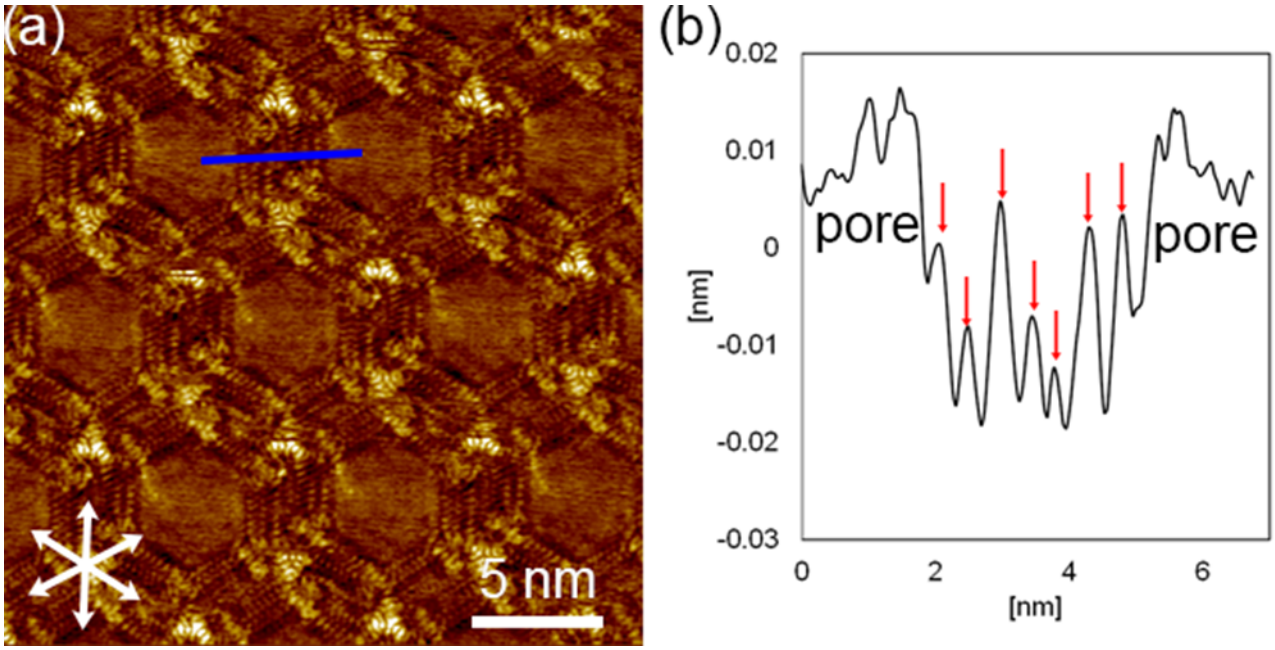

Fig. S3. (a) STM image of a hexagonal porous structure formed by **DBA-OC14-OH** (1.0×10^{-4} M, after annealing treatment, I_{set} = 100 pA, V_{bias} = –0.40 V) and (b) A representative line profile for cross section height analysis along the blue line in (a). Red arrows in (b) point to peak tops of the adsorbed alkyl chains.

2-3. STM Images of Chirality of Hexagonal Porous Structure

In the hexagonal porous structure, two chiral domains were observed (Figs. S4a,b).[11] This supramolecular chirality can be discerned by the clockwise (CW) or counter-clockwise (CCW) orientation of the alkyl chains located at the rims of the hexagonal pore (Figs. S4c,d). It is also expressed by the angle α between the unit cell vector and the normal $\langle 1\bar{1}00 \rangle$ to one of the main symmetric axes of graphite. The mean angles α determined at 50 points from several calibrated STM images are –5.7 ± 0.5° and 5.1 ± 1° for the CW and CCW structures, respectively.

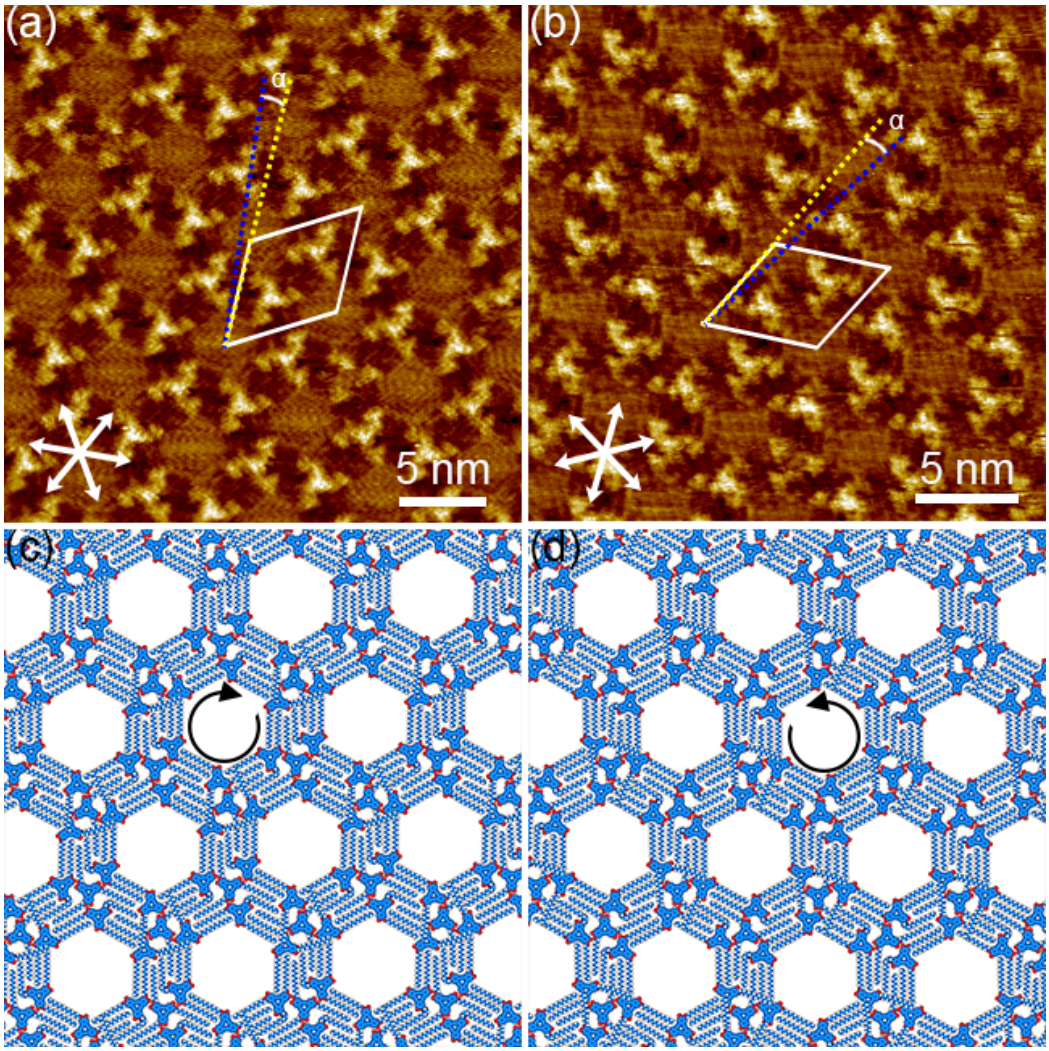

Fig. S4. STM images of (a) clockwise (CW) and (b) counterclockwise (CCW) hexagonal porous structures of **DBA-OC14-OH** at the TCB/graphite interface (conditions; (a) 3.0×10^{-6} M, I_{set} = 200 pA, V_{bias} = –0.40 V, and (b) 1.0×10^{-4} M I_{set} = 200 pA, V_{bias} = –0.40 V). White arrows in (a) and (b) indicate the orientation of the main symmetry axes $\langle 1\bar{1}00 \rangle$ of the graphite underneath. Blue and yellow dotted lines are the directions of the normal $\langle 1\bar{1}00 \rangle$ to one of the substrate's symmetry axes and one of the unit cell vectors, respectively. CW or CCW rotation of the unit cell vectors to the normal is expressed by + or − signs of the angle α, respectively. In this assignment, the angles α become negative and positive values for the CW and CCW domains. (c, d) Molecular models of CW and CCW hexagonal porous structures constructed by MM calculations.

2-4. Brightness of Central DBA Molecule

In the hexagonal porous structure, a central **DBA-OC14-OH** molecule in the tetramer was imaged brighter than the surrounding three **DBA-OC14-OH** molecules. The apparent height of the tetramers was analyzed from five calibrated STM images. A typical cross section height analysis along the blue line (11 pixels) in Fig. S5a is displayed in Fig. S5b. We performed the same analyses for 50 points and the apparent heights at each point (pixel) were averaged. The lowest point was set to 0 pm. The average apparent heights of the central and surrounding **DBA-OC14-OH** molecules in the tetramer were 117 ± 10 and 76 ± 7 pm, respectively (Fig. S5b). The average height of the central molecule is less than double of that of the surrounding DBAs. Note that the central **DBA-OC14-OH** molecule sometimes appears dim, where the average apparent height is close to the pore part (42 ± 8 pm, Fig. S6). No concentration dependency was observed for the number of such dim central DBA. The reason for the bright appearance of the central DBA is not clear yet, we consider that this might be due to the parallel stacked dimer formation or different registry of the DBA π-core to the substrate lattice.

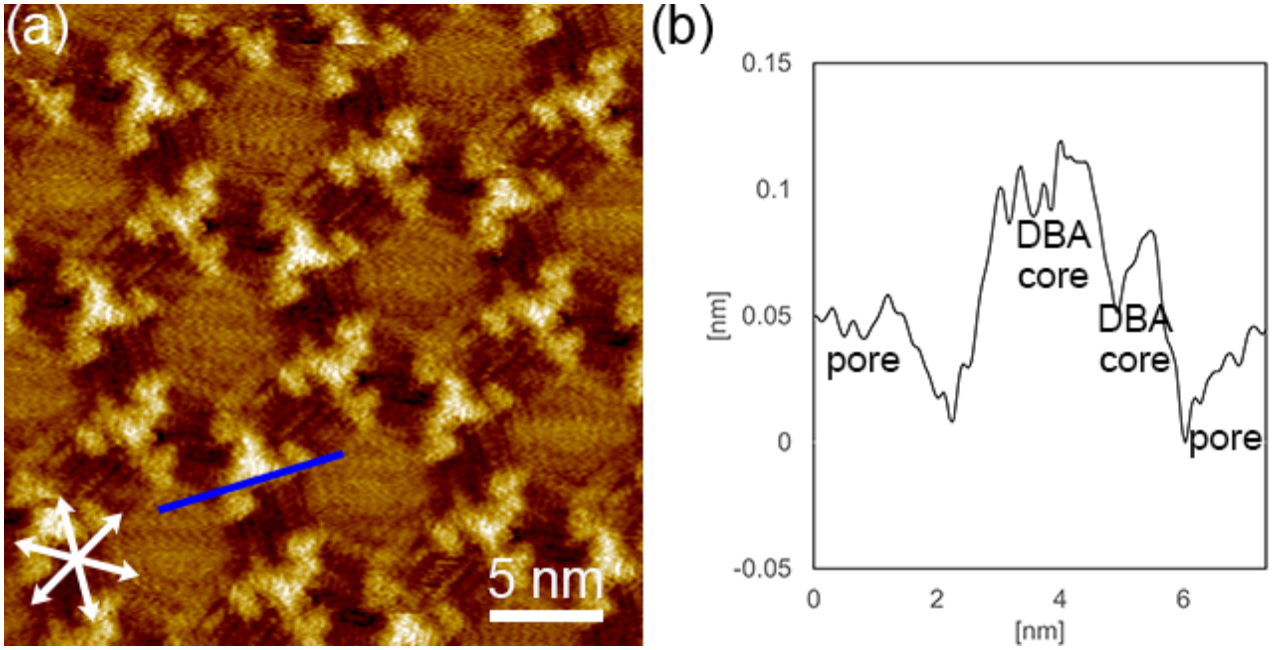

Fig. S5. STM image of a hexagonal porous structure formed by **DBA-OC14-OH** (3.0×10^{-6} M, I_{set} = 200 pA, V_{bias} = –0.40 V) and a representative cross section analysis along a blue line in image (a).

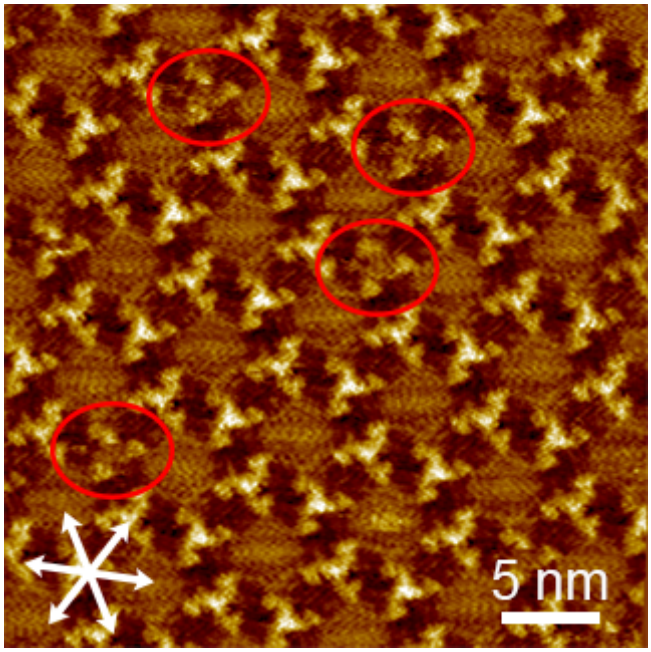

Fig. S6. STM image of a hexagonal porous structure with defects (3.0×10^{-6} M, I_{set} = 200 pA, V_{bias} = –0.40 V). Red ovals indicate the defects where the central DBA parts appear dim.

2-5. Construction of Molecular Models of Hexagonal Porous Structure

In the hexagonal porous structure, the seven alkoxy chains are interdigitated between the adjacent tetramers. At each side of the tetramer, the three or four alkoxy groups can participate in alkyl chain interdigitation with the adjacent cluster. A [3+4] type interaction in which the three and four alkoxy chains participate from each tetramer would be an optimal interaction mode. In the modeling, we assume that the triangular tetramer consists of a C_{3h}-symmetric central molecule (Fig. S7a) and C_1- and/or C_s-symmetric surrounding molecules (Figs. S7b, c). The one or two alkoxy group(s) in the latter two geometries orient to the solution phase (m = 1 or 2). There are four possible tetramers by combining the central C_{3h}-symmetric molecule and surrounding three C_1- and/or C_s-symmetric molecules, as follows; (C_1, C_1, C_1), (C_s, C_s, C_s), (C_1, C_1, C_s) and (C_1, C_s, C_s) tetramers. Since the seven interdigitated alkoxy chains were observed, only two combinations of (C_1, C_1, C_1)/(C_s, C_s, C_s) and (C_1, C_1, C_s)/(C_1, C_s, C_s) are possible (Fig. S8). Among these two possible structures, we analyzed structure parameters, *i.e.,* O···H interatomic distances only for the (C_1, C_1, C_1)/(C_s, C_s, C_s) model, as this is more stable, yet the difference is very small, than the (C_1, C_1, C_s)/(C_1, C_s, C_s) model by the MM calculations (0.036 kcal·mol^{-1}·nm^{-2}, Figs. S8a and b).

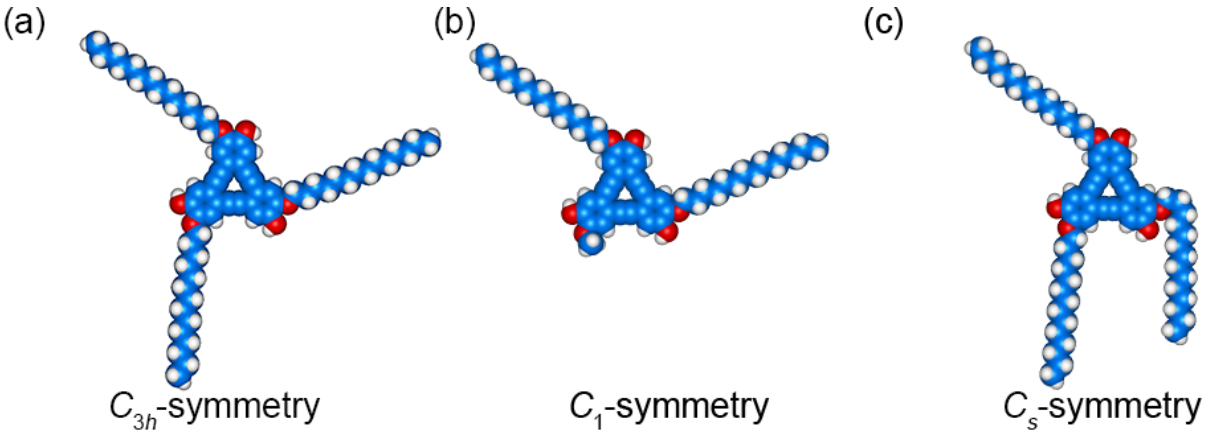

Fig. S7. Three optimized molecular models of **DBA-OC14-OH** with (a) C_{3h}- (m = 3), (b) C_1- (m = 2) and (c) C_s- (m = 3) symmetric geometries by MM calculations. In the molecular models in (b), a desorbed alkoxy group is replaced with a methoxy group.

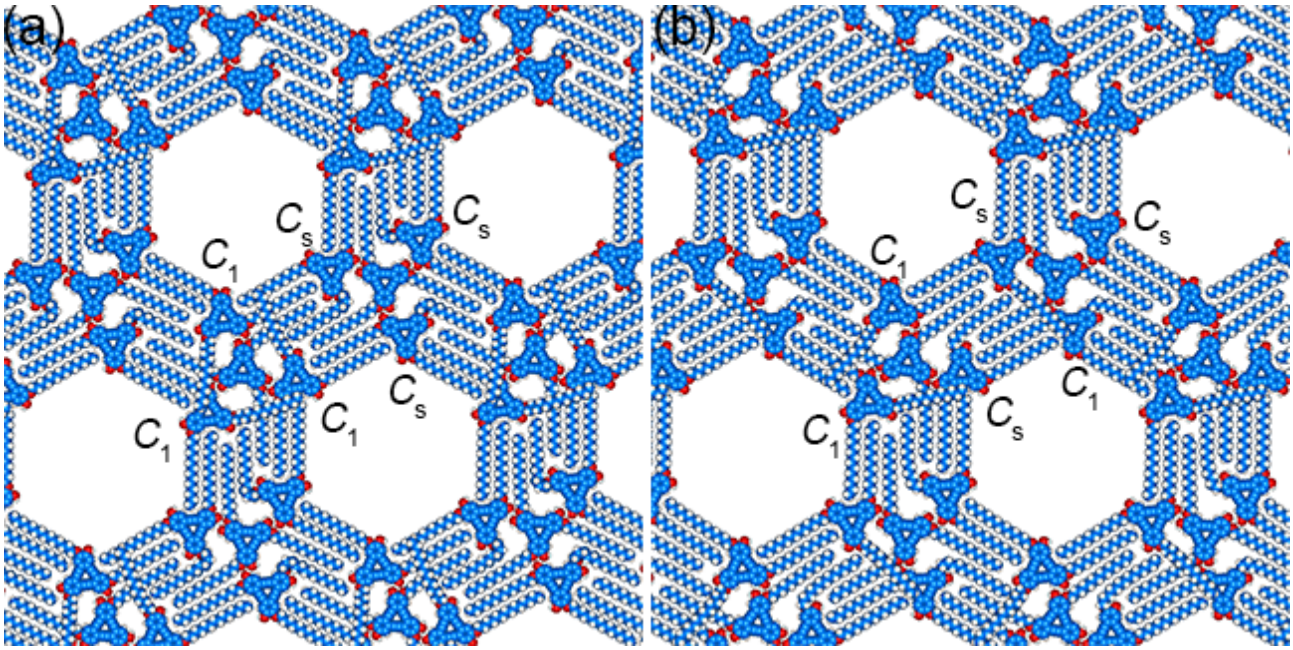

Fig. S8. Molecular models of the hexagonal porous structures composed of (a) (C_1, C_1, C_1)/(C_s, C_s, C_s) and (b) (C_1, C_1, C_s)/(C_1, C_s, C_s) geometries constructed by MM calculations.

2-6. Chirality of Hexagonal Porous Structure

In the hexagonal porous structures, there are both point and supramolecular chirality.[12,13] At a single molecular level, the chirality is differentiated by the substitution pattern, *i.e.* the alkyl chains are attached to the right or left oxygen atoms of each benzene ring of **DBA-OC14-OH**. The former and latter are referred to as *R*- and *S*-type enantiomers, respectively. Given that the hexagonal porous structure consists of (C_1, C_1, C_1)/(C_s, C_s, C_s) tetramers, both enantiomers constitute the tetramer, in which the chirality of the central DBA is opposite from that of the surrounding three molecules. For example, when the central molecule is *R*-type, the surrounding three DBAs are *S*-type. This tetramer is denoted as *R*-3*S*-teramer. The antipodal tetramer is *S*-3*R*-teramer. This chirality switching is essential to form hydrogen bonding between the DBAs and avoid sterically unfavorable alkyl chain orientation. The supramolecular chirality at the hexagonal porous structure level, clockwise (CW) or counterclockwise (CCW) rotation, can be differentiated by the orientations of the alkyl chains at the rims of the hexagonal pore. The CW hexagonal porous structure consists of the *S*-3*R*-tetramers, while the CCW structure consists of the *R*-3*S*-tetramers, to form optimal [3+4] interaction mode between the tetramers.

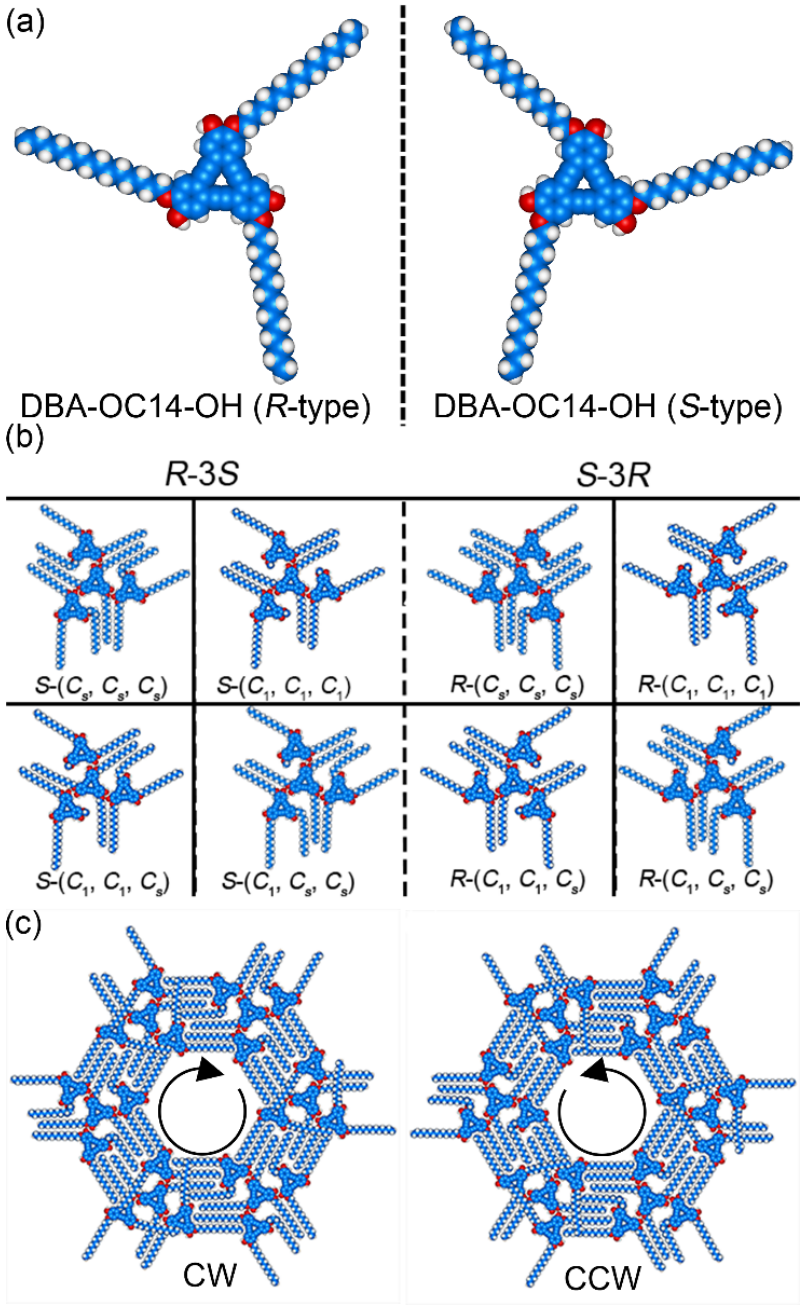

Fig. S9. Chiral hexagonal porous structures formed by **DBA-OC14-OH**. (a) On-surface point chirality (*S*- or *R*-type) of **DBA-OC14-OH** at a single molecular level. (b) Supramolecular chirality at the tetramer level (*S*-3*R*- or *R*-3*S*-tetramers). There are eight possible tetramers consisting of different chiral geometries at a single molecular level. (c) Supramolecular chirality at the hexagonal porous structure level (clockwise (CW) and counterclockwise (CCW) rotations). In the molecular models (b, c), the desorbed alkoxy groups are replaced by the methyl groups.

3. Self-Assembly of DBA-OC14-OH at the HA/Graphite Interface

3-1. Additional STM Images

From the STM images shown in Fig. S10, four long alkyl chains of **DBA-OC14-OH** and two short alkyl fragments (red dotted ovals) were discerned between two adjacent clusters. We attribute these short alkyl fragments to co-adsorbed solvent HA molecules.

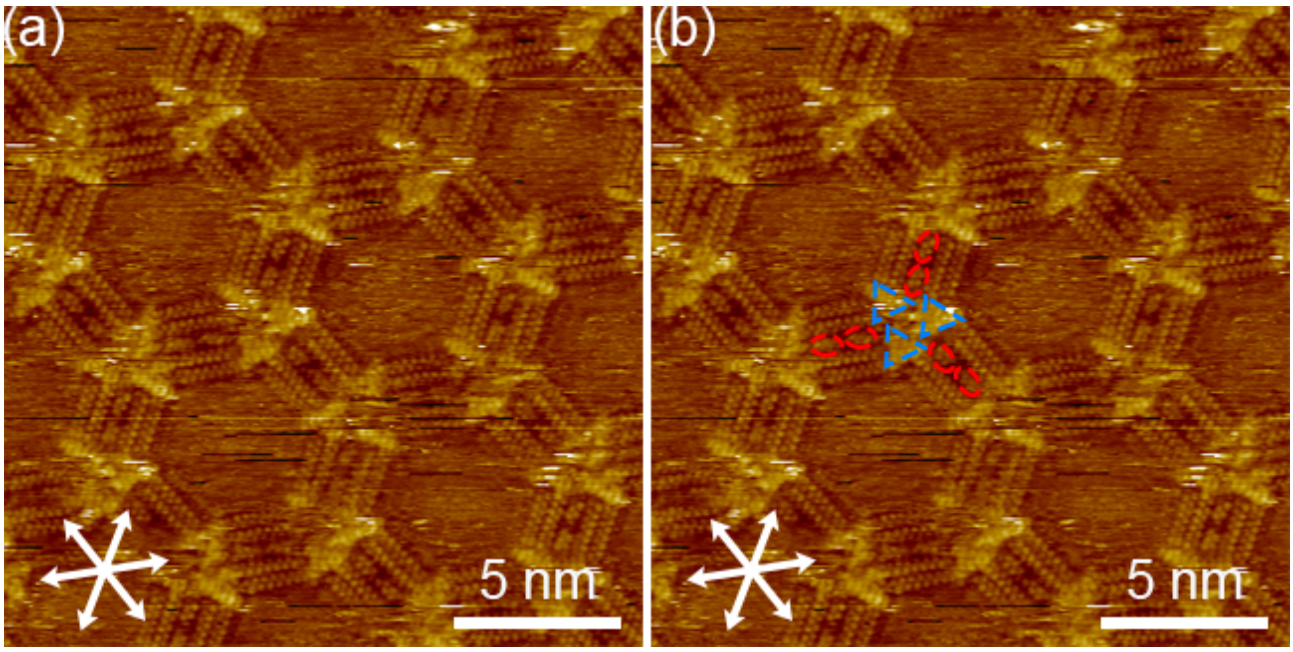

Fig. S10. (a, b) STM images of a triangular cluster (n = 2) structure formed by **DBA-OC14-OH** (6.0 × 10^{-6} M, I_{set} = 200 pA, V_{bias} = –0.79 V) at the HA/graphite interface. Blue dotted triangles and red dotted ovals in (b) are the DBA π-cores of the trimers and co-adsorbed HA molecules, respectively.

3-2. Construction of Molecular Models of Triangular Cluster (n = 2) Structure

There are two possible geometries for the co-adsorbed HA molecules, one forming a hydrogen bonded carboxylic acid dimer (a head-to-head interaction mode) and the other forming heteromolecular hydrogen bonds with the hydroxy groups of **DBA-OC14-OH** (a tail-to-tail interaction mode). Comparison of the stabilization energies (E_{total}) of the two geometries supports that

the latter geometry is stable over the former by 1.2 kcal·mol^{-1}·nm^{-2} (Figs. S11a and b). Hereafter we assume that the carboxyl group of HA is hydrogen bonded to the hydroxy groups of the DBA.

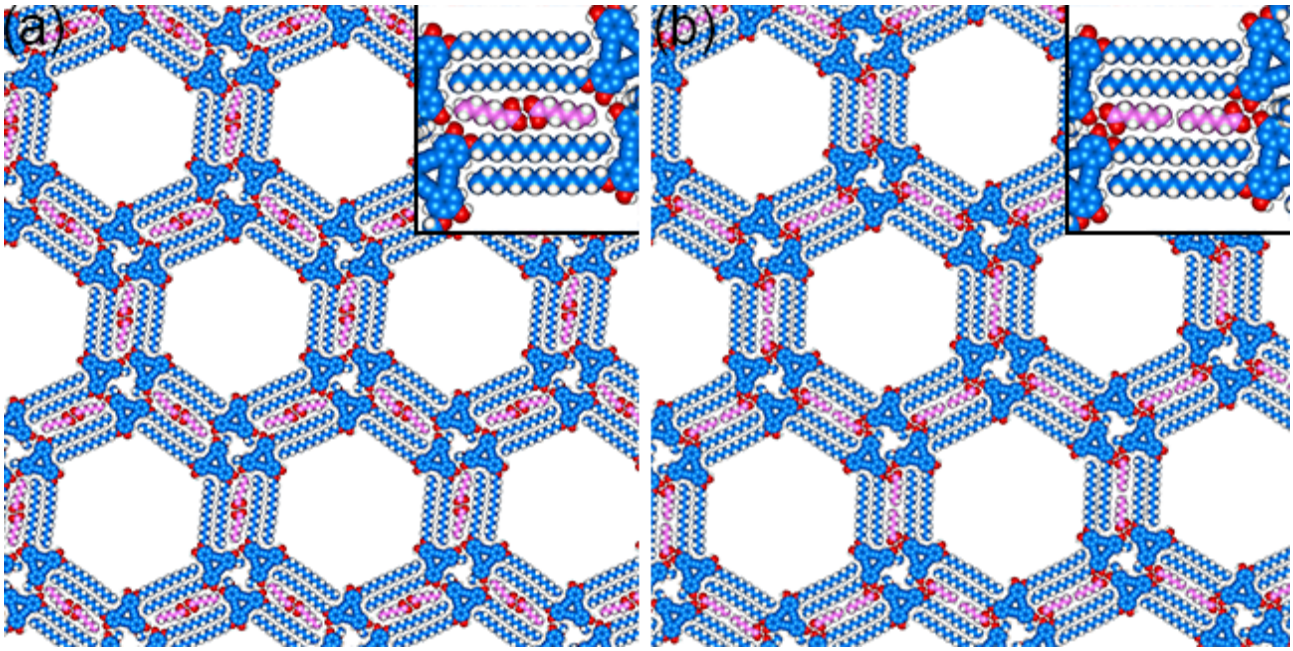

Fig. S11. Molecular models constructed by MM calculations. (a) Triangular cluster (n = 2) with the carboxylic acid dimer (the head-to-head interaction). (b) Triangular cluster (n = 2) with the heteromolecular hydrogen bonding interaction between HA and **DBA-OC14-OH** molecules (the tail-to-tail interaction). Co-adsorbed HA molecules are colored in magenta. For models (a) and (b), one OC14 group per a single DBA molecule is replaced by methoxy group to represent the alkoxy group orienting to the solution phase.

3-3. Chirality of Triangular Cluster Structure

Chirality of the Triangular cluster is also expressed both at single molecular and supramolecular levels. At a single molecular level, chirality (*R*- or *S*-type) can be differentiated by the substitution patterns too (Fig. S12a). Assembly of three homochiral enantiomers forms chiral trimers (*R*-*R*-*R*- or *S*-*S*-*S*-trimers, Fig. S12b). The supramolecular chirality (clockwise (CW) or counter-clockwise (CCW) rotation) is discerned by the orientations of the alkoxy chains at the rims

of the pore (Fig. S12c). The CW and CCW structures are composed of the *R*-*R*-*R*- or *S*-*S*-*S*-trimer, respectively.

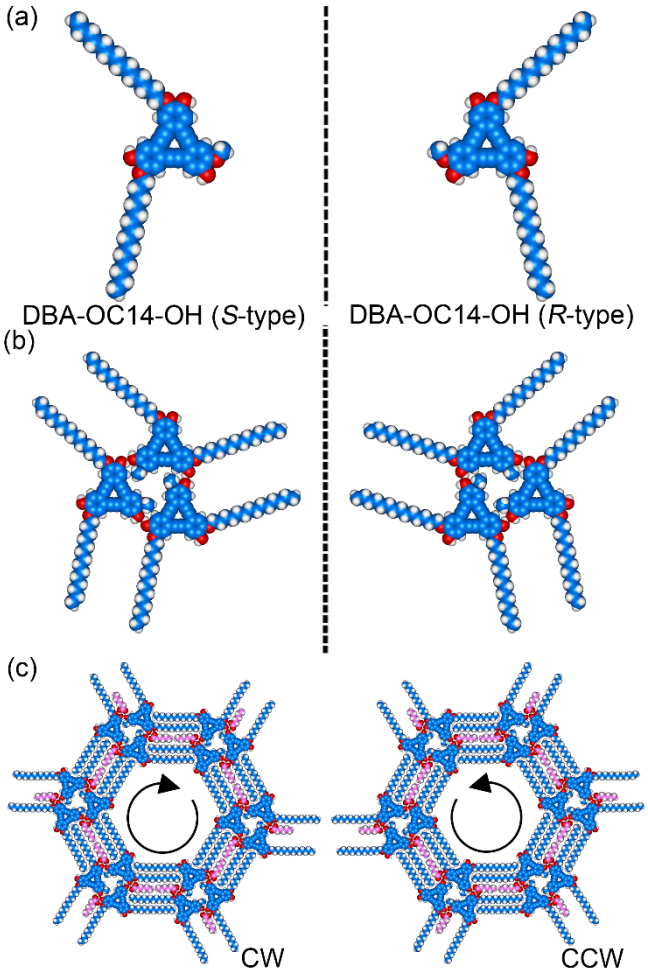

Fig. S12. Molecular models for chiral triangular cluster (n = 2) formed by **DBA-OC14-OH**. (a) On-surface chirality of **DBA-OC14-OH** at a single molecular level. (b) Chirality of the trimer of **DBA-OC14-OH**. (c) Chirality of the triangular cluster (n = 2, clockwise (CW) and counterclockwise (CCW)). In the molecular models, the desorbed alkoxy groups are replaced with methyl groups.

Supramolecular chirality at the pore level is also distinguished by the angle α between one of the unit cell vectors of the CW and CCW structures and the normal $\langle 1\bar{1}00 \rangle$ to one of the main axes of graphite. We measured more than 50 points from five calibrated STM images (30 × 30 nm^2 or smaller). As a result, the average angles α were –5.0 ± 0.6° and 5.0 ± 0.5° for the CW and CCW structures (Figs. S13a, b).

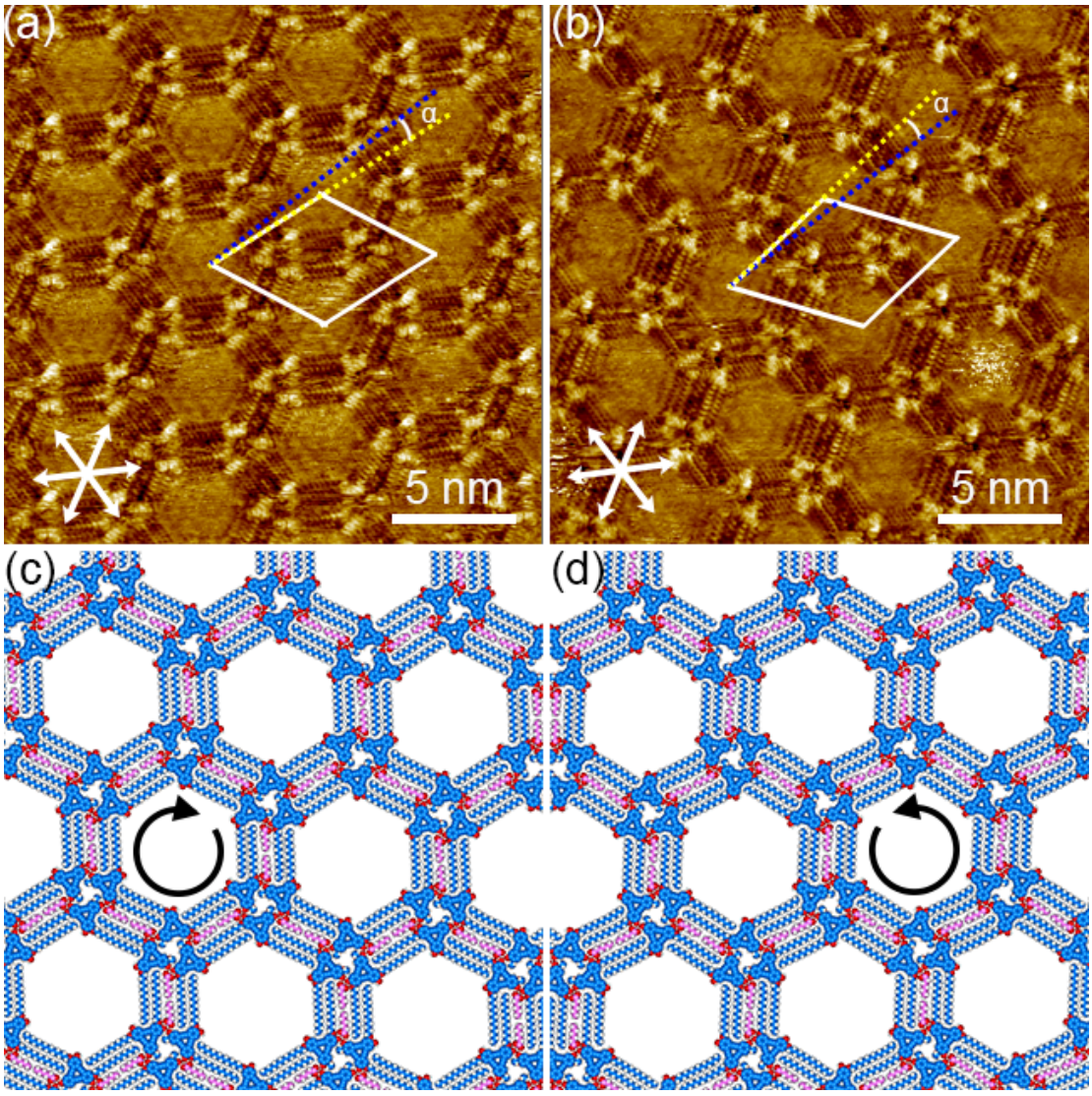

Fig. S13. STM images of (a) clockwise (CW) and (b) counterclockwise (CCW) triangular clusters (n = 2) of **DBA-OC14-OH** at the HA/graphite interface (conditions; (a) 1.0 × 10^{-4} M, I_{set} = 200 pA, V_{bias} = –0.40 V, and (b) 1.0 × 10^{-4} M, I_{set} = 200 pA, V_{bias} = –0.40 V). White arrows in images (a) and (b)

indicate the main symmetry axes ⟨1$\bar{1}$00⟩ of the graphite underneath. Light blue and yellow dotted lines are directions of the normal ⟨1$\bar{1}$00⟩ to one of the substrate's symmetry axes and one of the unit cell vectors, respectively. Clockwise (CW) or counterclockwise (CCW) rotation of the unit cell vectors to the normal is expressed by + or − signs of the angle α, respectively. (c, d) Molecular models of the CW and CCW triangular clusters (n = 2) constructed by MM calculations. Co-adsorbed HA molecules are colored in magenta. For models (c) and (d), one OC14 group is replaced by methoxy groups to represent the alkoxy group orienting to the solution phase.

3-4. Co-Existence of Various Structures at Middle Concentration Range

At the HA/graphite interface, **DBA-OC14-OH** forms a disordered structure at the middle concentration range (1.0×10^{-5} M). The triangular clusters with various sizes (n = 2 to 6) co-exist without regularity together with the domains of the dense structures. The small domains of the triangular cluster (n = 2) ca. 50×50 nm^2 were sometimes observed.

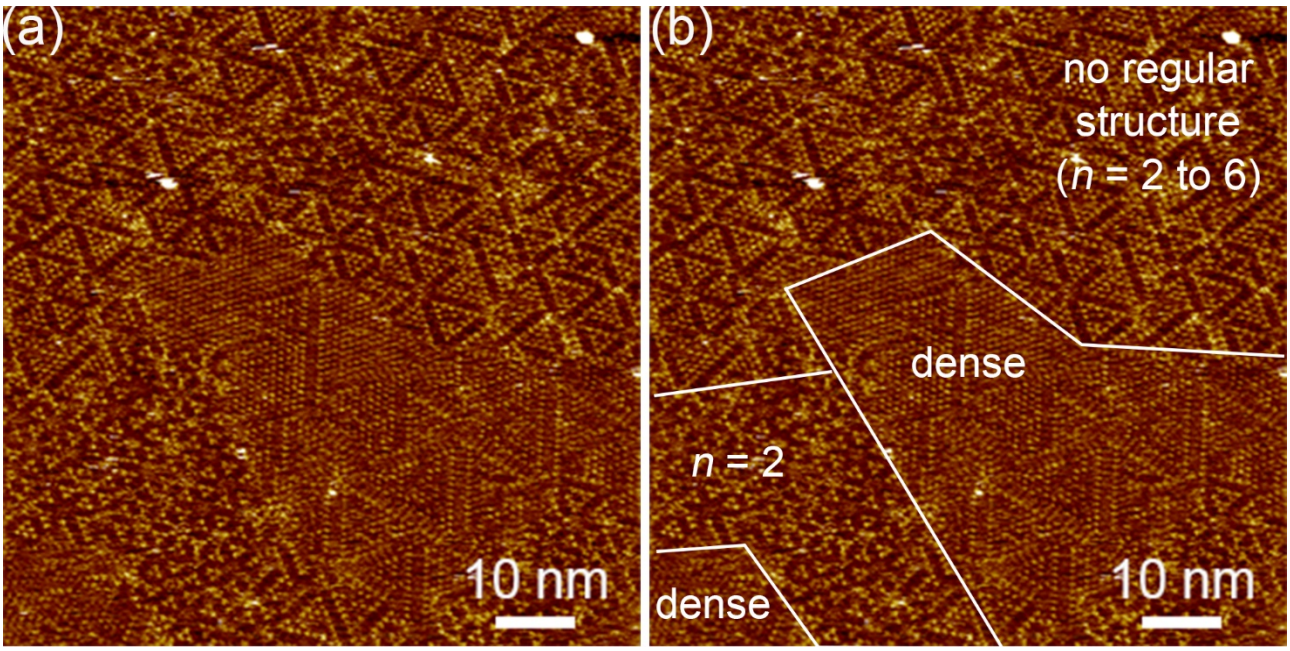

Fig. S14. (a) Large STM image at the HA/graphite interface including various structures (conditions; 1.0×10^{-5} M, I_{set} = 250 pA, V_{bias} = –0.40 V). (b) The same image as (a) with white lines indicating domain boundaries and structure assignments for each domain.

3-5. Additional STM Images of Dense Structure

In several STM images, chirality of the dense structure is also assigned at both single molecule and supramolecular levels (Fig. S15). The single molecular chirality (*R*- or *S*-type) is transferred to a supramolecular level. This chirality is domain specific. While the boundaries between antipodal domains are disordered in most of cases, the homochiral domains are occasionally connected through interdigitated alkyl chains at the boundary (indicated by a red dotted rectangle in Fig. S15b).

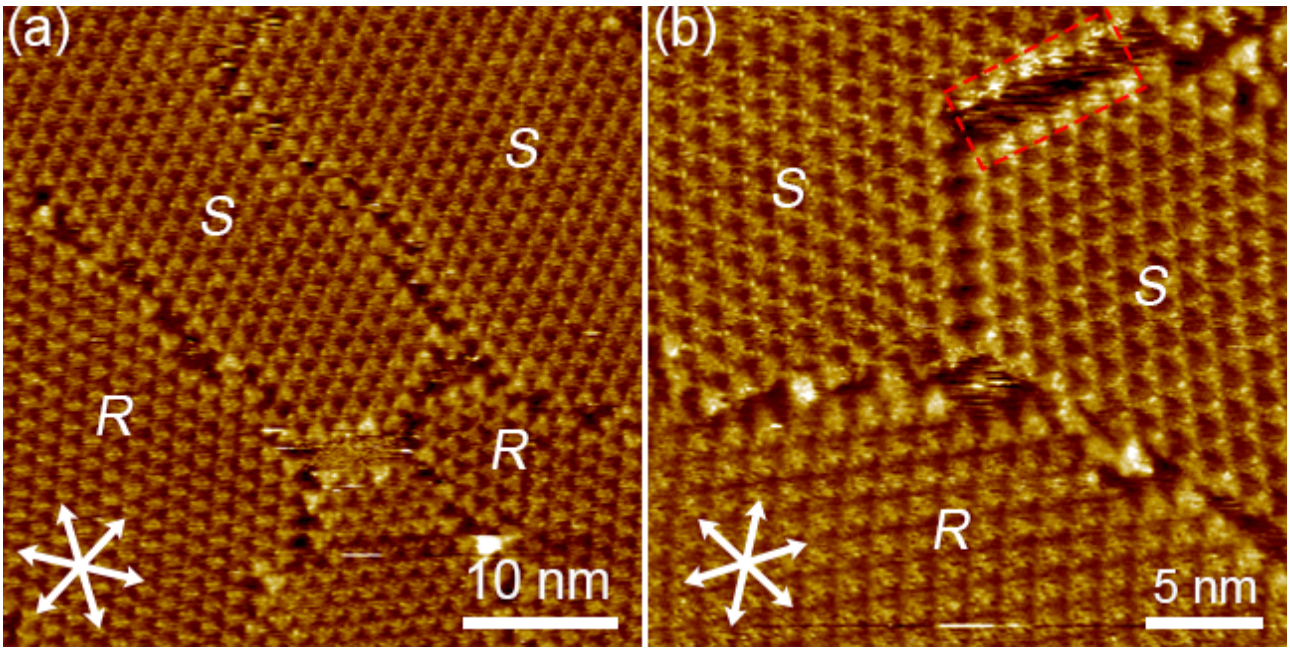

Fig. S15. (a, b) STM images of the dense structure (conditions; 1.0×10^{-4} M, I_{set} = 250 pA, V_{bias} = –1.12 V). Chirality of each domain is indicated by *R* or *S*. Red dotted rectangle in (b) indicates interdigitated alkyl chain parts at the domain boundary.

3-6. Molecular Models and Chirality of Dense Structure

In the STM images of the dense structure, only π-cores of **DBA-OC14-OH** were imaged, indicating that all alkyl chains orient to the solution phase. Chiral structural models of the dense structure are optimized by MM calculations using the experimentally derived unit cell parameters under the PBC conditions (Fig. S16).

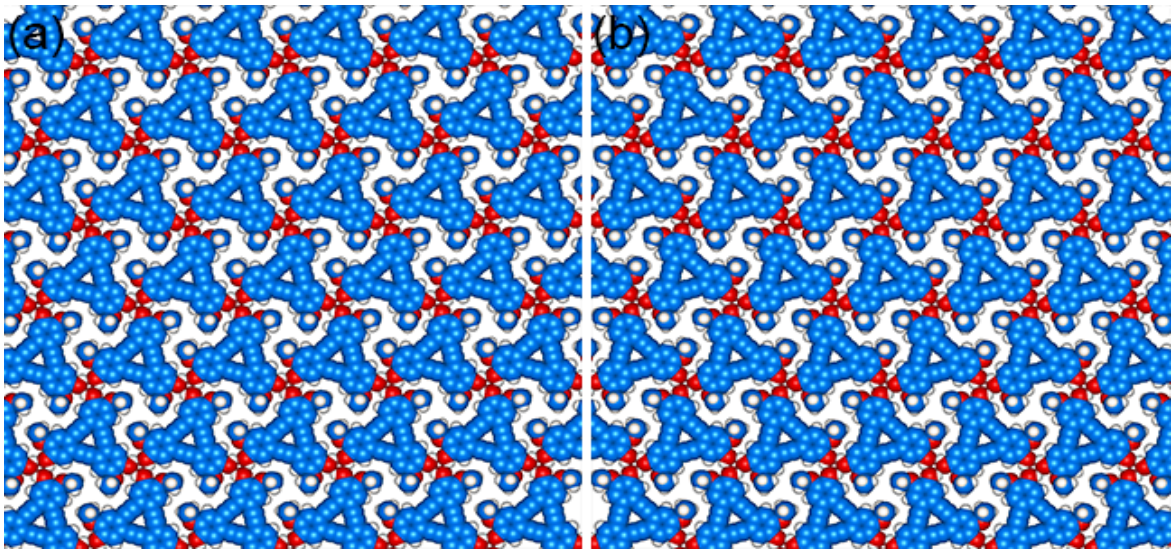

Fig. S16. Molecular models constructed by MM calculations. (a) Dense structure formed by *S*-type **DBA-OC14-OH**. (b) Dense structure formed by *R*-type **DBA-OC14-OH**. In (a, b), the desorbed alkoxy groups are replaced with methyl groups.

4. Self-Assembly of DBA-OC14-OH at the TCB-HA Mixture/Graphite Interface

4-1. STM Images Formed at X_{HA} = 0.02 to 0.082

Solutions in mixtures of TCB and HA of the HA molar fraction (X_{HA}) ranging from 0.02 to 0.50 were prepared keeping the concentration of **DBA-OC14-OH** to 1.0×10^{-4} M (the highest value in this study). Using these solutions, STM measurements were conducted at the liquid/graphite interface. The results are summarized in Table 1.

At the lowest X_{HA} value (0.020), there are both a hexagonal porous structure and a triangular cluster (n = 2, Fig. S17a). At X_{HA} of 0.049–0.066, **DBA-OC14-OH** mainly forms a triangular cluster (n = 2) similar to the pure HA system at low concentration (Fig. S17b). Upon increasing X_{HA} to 0.070–0.082, a larger triangular cluster (n = 4) appears which extends to form domains of the size over 80 × 80 nm^2 together with the domains of the smallest triangular cluster (n = 2, Figs. S17c,d). At X_{HA} of 0.082, in addition to the extensive domains of the triangular clusters (n = 2 and 4, Figs.

S18c and d), the domain of large triangular clusters ($6 < n < 15$) was observed only once, which is displayed in Figs. S18a,b.

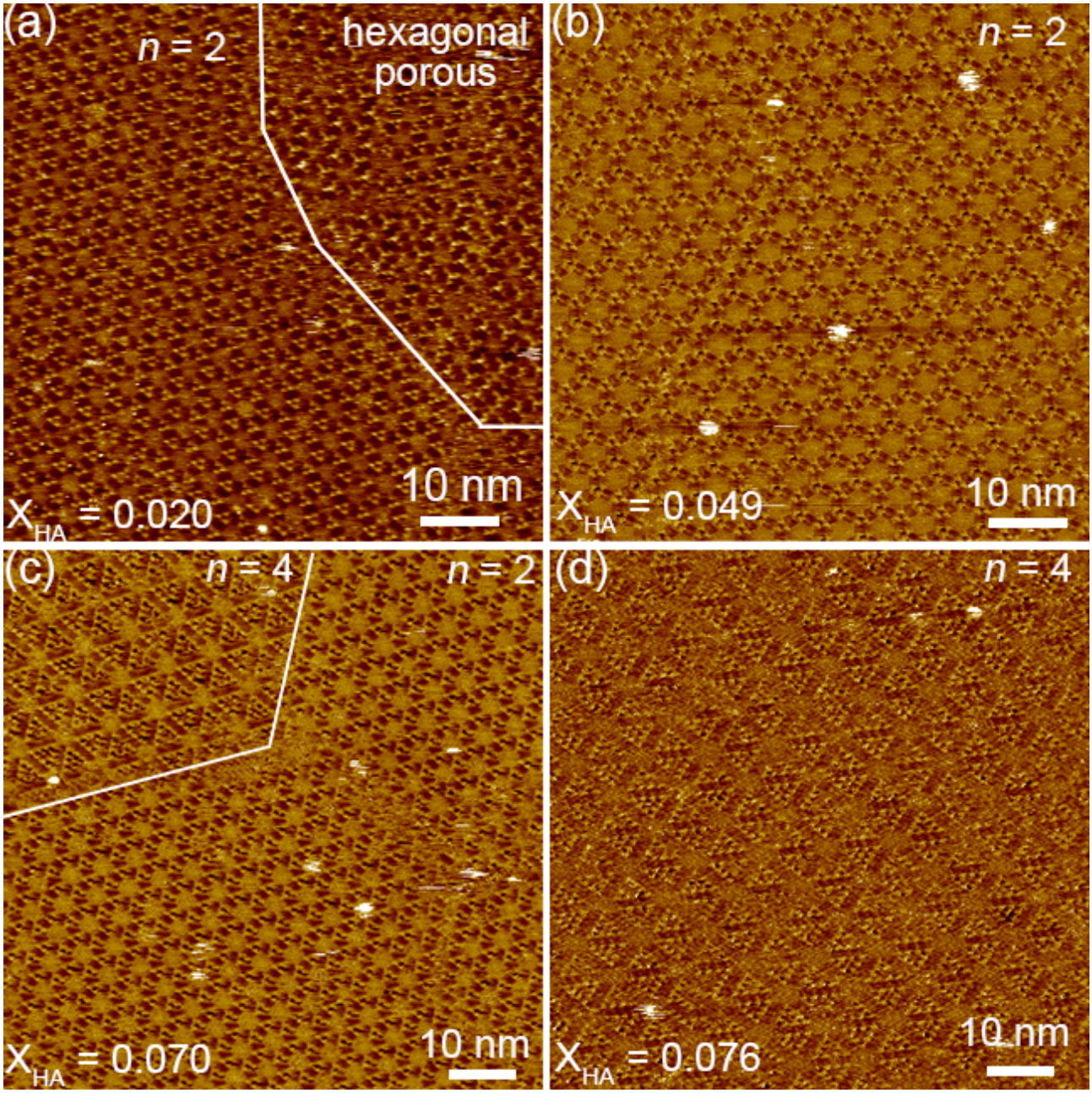

Fig. S17. STM images of the triangular clusters at the TCB-HA/graphite interface. (a) Triangle cluster ($n = 2$) and hexagonal porous structure at $X_{HA} = 0.020$ ($I_{set} = 200$ pA, $V_{bias} = -0.40$ V). (b) Triangular cluster ($n = 2$) at $X_{HA} = 0.020$ ($I_{set} = 200$ pA, $V_{bias} = -0.40$ V). (c) Triangular clusters ($n = 2$ and 4) at $X_{HA} = 0.070$ ($I_{set} = 200$ pA, $V_{bias} = -0.40$ V). (d) Triangular cluster ($n = 4$) at $X_{HA} = 0.076$ ($I_{set} = 200$ pA, $V_{bias} = -0.40$ V).

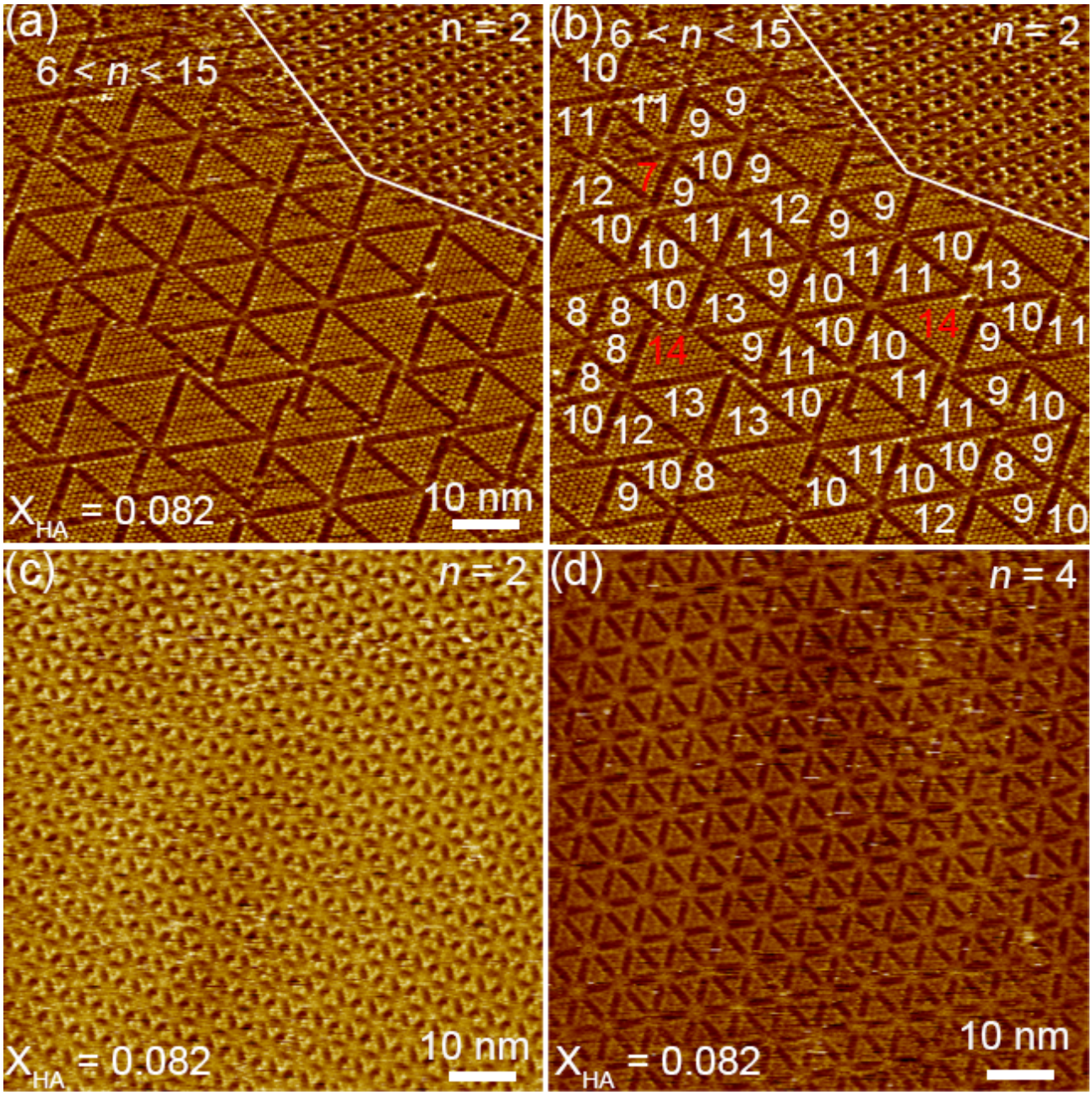

Fig. S18. STM images of the triangular clusters at the TCB-HA/graphite interface (X_{HA} = 0.082). (a) Area of triangular clusters of n = 2 and 6 < n < 15 together with defects between the large clusters (I_{set} = 200 pA, V_{bias} = –0.40 V). (b) The same image as (a) in which the sizes (n) of the triangle clusters are indicated. The clusters with red numbers partially collapse due to large size mismatches with the adjacent clusters. (c) Area of triangular cluster (n = 2, I_{set} = 200 pA, V_{bias} = –0.40 V). (d) Area of triangular cluster (n = 4, I_{set} = 200 pA, V_{bias} = –0.40 V).

4-2. Enlarged STM Images of Triangular Cluster (n = 4)

At the TCB-HA/graphite interface, **DBA-OC14-OH** forms hexagonally packed triangle clusters (n = 4) at X_{HA} ranging from 0.070 to 0.090. The triangular cluster is most likely composed of ten **DBA-OC14-OH** molecules, although the central **DBA-OC14-OH** molecule is not always visualized. The eight alkyl chains of **DBA-OC14-OH** and six short alkyl units of HA (red dotted ovals) are observed between the adjacent clusters (Fig. S19). The unit cell parameters of the triangular cluster (n = 4) are a = b = 9.2 ± 0.2 nm and γ = 60 ± 1°.

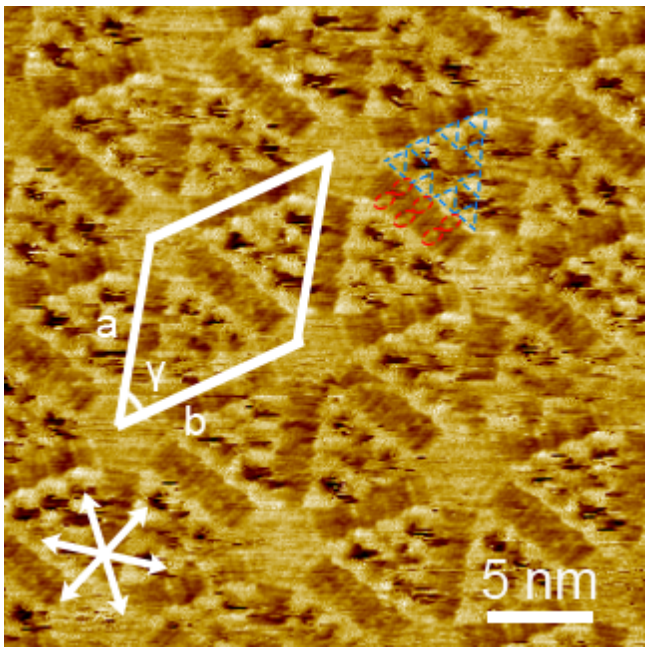

Fig. S19. STM image of a triangular cluster of n = 4 formed by **DBA-OC14-OH** at the TCB-HA/graphite interface at X_{HA} = 0.076 (I_{set} = 300 pA, V_{bias} = –0.46 V). Light blue dotted triangles and red dotted ovals are the DBA π-cores and co-adsorbed HA molecules, respectively.

4-3. Construction of Molecular Models of Triangular Cluster (n = 4)

On the basis of the unit cell parameters of the triangular cluster (n = 4), a model is optimized by the MM calculations (Fig. S20a). In the model, mean interatomic O···H distances between the hydroxy group of **DBA-OC14-OH** and HA (Fig. S20b) and between the hydroxy groups of **DBA-**

OC14-OH (m = 2 and 1) at the periphery of the cluster (Fig. S20c) are 1.78 ± 0.02 and 1.80 ± 0.02 Å, respectively (Fig. S20b). The distance between the hydroxy groups between the DBA of m = 0 is 1.83 ± 0.03 Å (Fig. S20c).

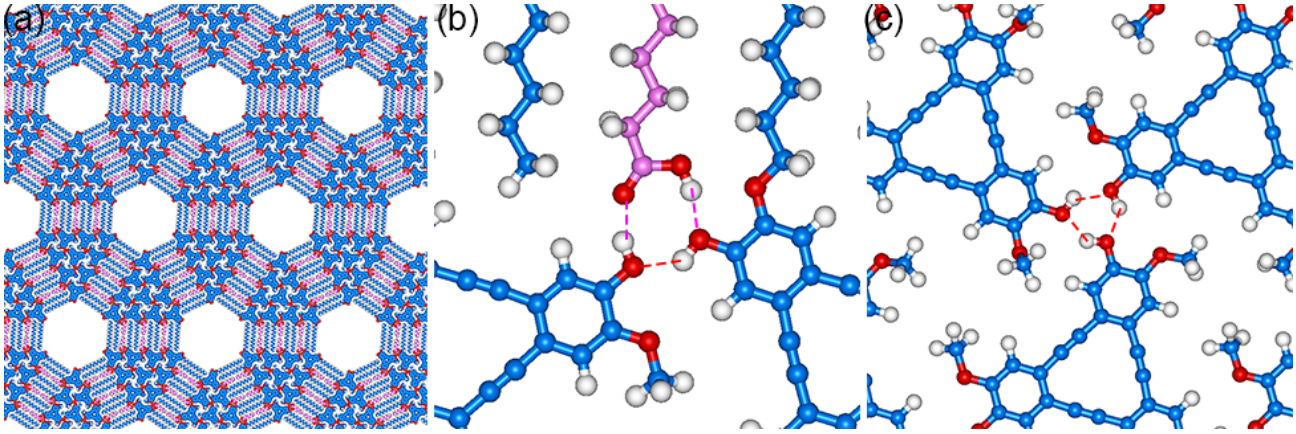

Fig. S20. Molecular models constructed by MM calculations. (a) Triangular cluster (n = 4). (b, c) Enlarged views of the hydrogen bonding sites. Interatomic O···H distances between **DBA-OC14-OH** (m = 2 and 1) and HA or between **DBA-OC14-OH**s are indicated by pink and red dotted lines respectively. The desorbed alkoxy groups are replaced with the methyl groups.

4-4. STM Images Formed at X_{HA} = 0.090

At X_{HA} ranging from 0.090, triangular clusters of n = 2 and 4 appear as extended domains over 80 × 80 nm^2 (Figs. S21a,b). In addition, larger triangular clusters of n = 6–14 were observed (Figs. S21b,c). Note that the domains of smaller clusters of n = 2 and n = 4 are separated from those containing larger clusters of $5 < n$, presumably due to large mismatching in the cluster sizes. We note that the domains of the larger triangular clusters of $5 < n < 15$ often rearrange to the smaller triangular clusters of n = 2 and 4 during scanning with STM tip. This observation implies that the larger triangular clusters of $5 < n < 15$ are metastable under the given experimental conditions.

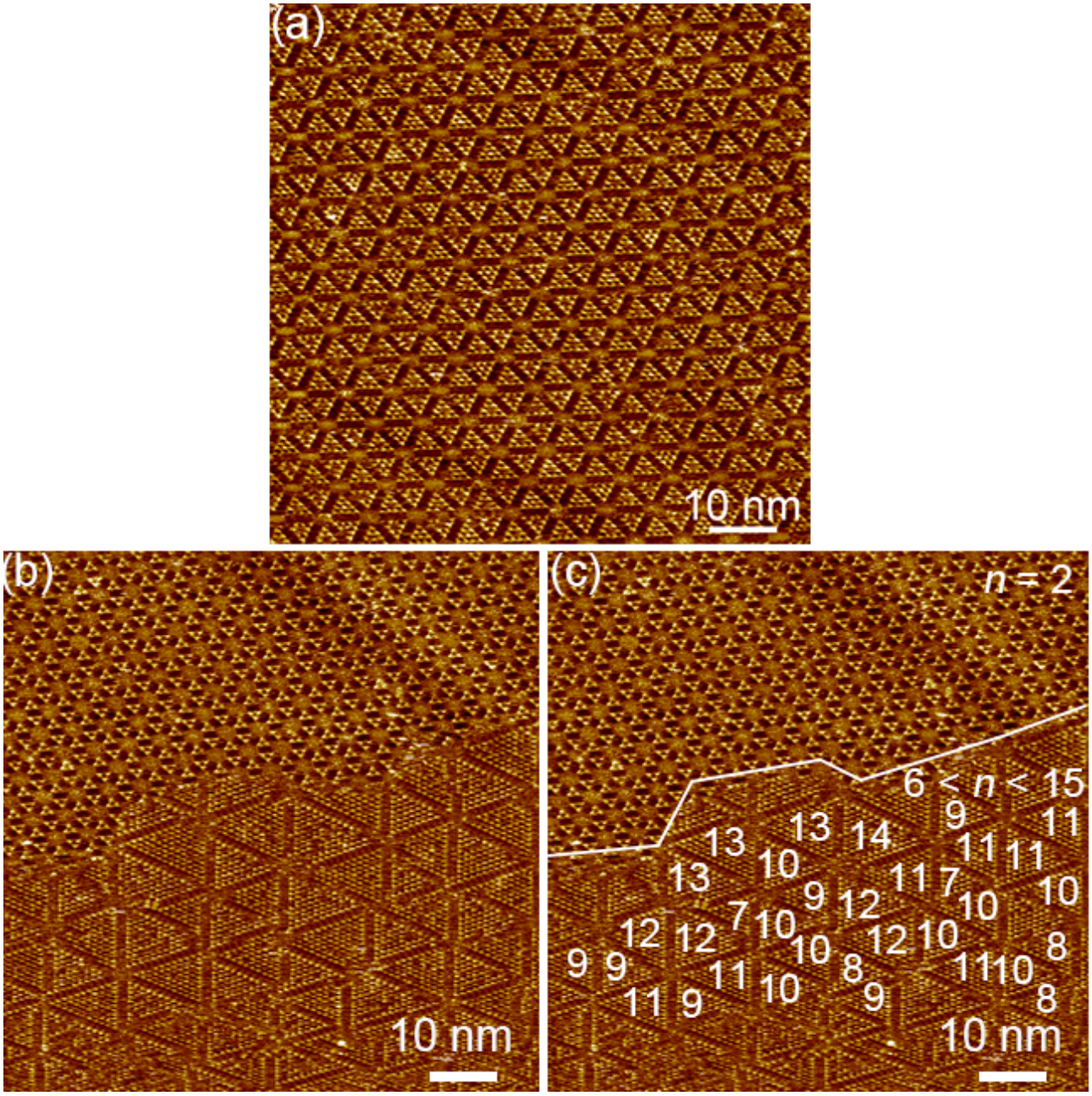

Fig. S21. STM images of the triangular clusters at the (mixture of HA and TCB)/graphite interface at X_{HA} = 0.090. (a) Area of triangular cluster (n = 4, I_{set} = 250 pA, V_{bias} = –0.40 V). (b) Triangular clusters of n = 2 and > 6 (I_{set} = 200 pA, V_{bias} = –0.40 V) (c) The same image as (b) with white line showing the boundary between domains of n = 2 and 6 < n < 15. The same image as (b) in which the sizes (n) of the triangle clusters are indicated.

4-5. Monolayers at X_{HA} of 0.2

As shown in Figs. 5a,b in the main text, at X_{HA} = 0.20, **DBA-OC14-OH** produces a large triangular cluster of n = 12 together with those having similar sizes (n = 10, 11, 13 and 14). The size distribution of the cluster is summarized in Table 2. These triangular clusters are arranged in a hexagonal manner forming a hierarchical long-range structure with a distorted hexagonal pore at the center unlike the smaller triangular clusters (n = 2 and 4). This is essential to keep the hexagonal packing. Bright triangular features were occasionally observed in the hexagonal pores (Fig. S22c), that were most probably attributed to co-adsorbed **DBA-OC14-OH** molecules. The alkyl chains are adsorbed between the large triangular clusters. The domains consisted of the large triangular clusters extend over 100 × 100 nm^2, yet n is not uniformed (Fig. S22b). These domains are stable against STM tip scanning contrary to the observation at X_{HA} = 0.090 (vide supra). Moreover, longer annealing period from 3 to 6 h led to no notable structural change. The hierarchical structure remains even after 1 day at room temperature. Based on these experimental observations, the domains of the hierarchical long-range structure are thermodynamically stable at this mixing ratio.

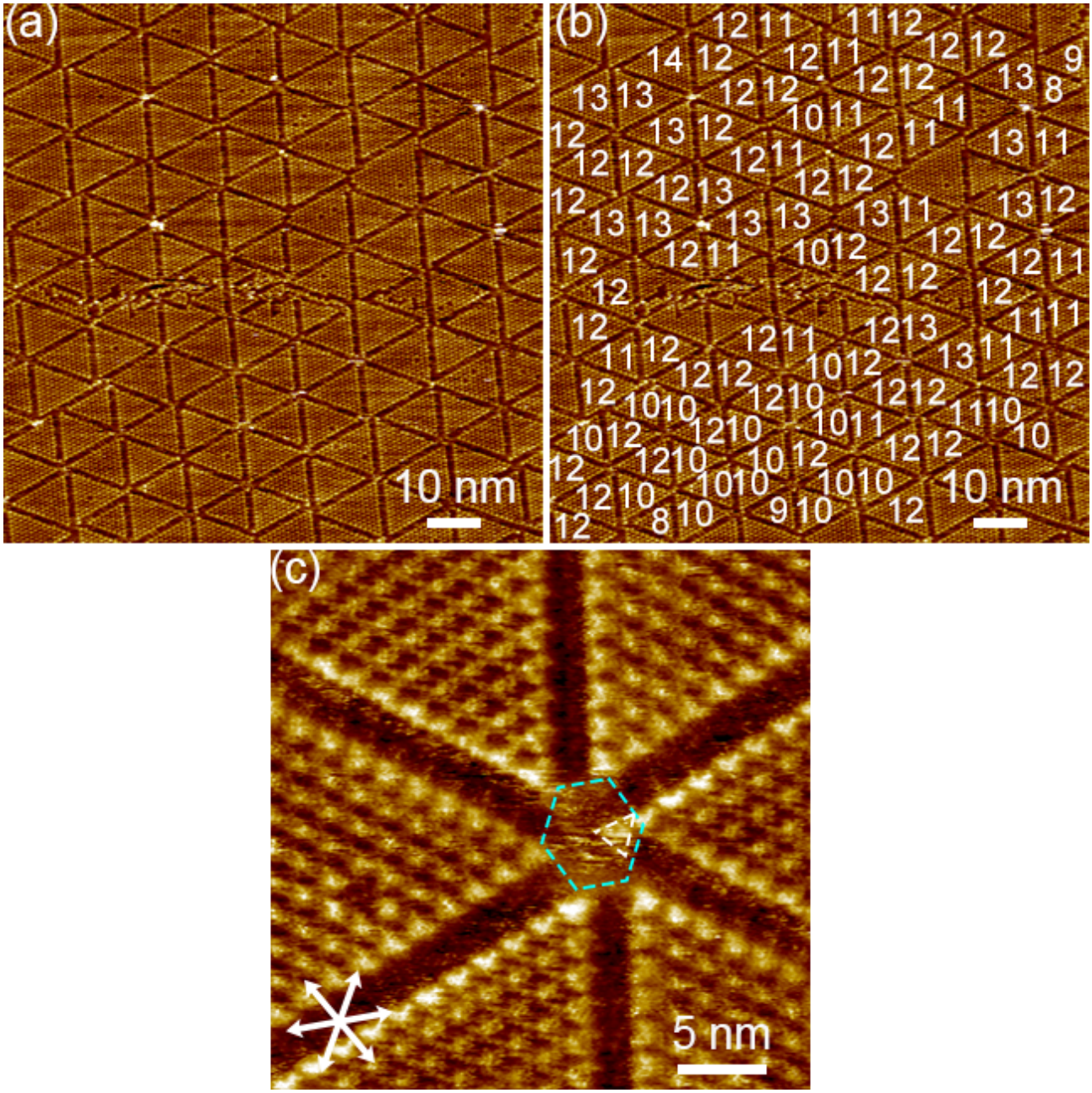

Fig. S22. STM images of a hierarchical triangular cluster packing observed at X_{HA} = 0.20. (a) Large domains of triangular clusters of n = 10–14 (I_{set} = 200 pA, V_{bias} = –0.40 V). (b) The same image as (a) in which the sizes (n) of the triangle clusters are indicated. (c) Enlargement at the hexagonal pore part (I_{set} = 200 pA, V_{bias} = –0.40 V). Turquoise dotted hexagon and white dotted triangle are the hexagonal pore and co-adsorbed DBA molecule, respectively.

4-6. Monolayers at X_{HA} from 0.5

At X_{HA} of 0.50, **DBA-OC14-OH** forms a dense structure with collapsed triangular clusters. A clear difference with the hierarchical triangular clusters observed at X_{HA} of 0.20 is no presence of hexagonal pores in SAMNs (Fig. S23). Moreover, between the structural boundaries, the alkyl chains were not observed in some parts.

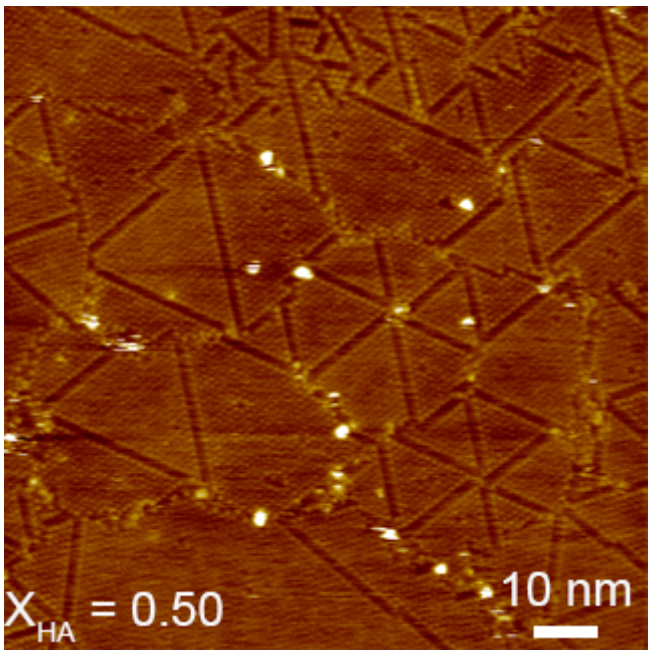

Fig. S23. STM image of the dense and collapsed triangular clusters at X_{HA} = 0.50 (I_{set} = 200 pA, V_{bias} = –0.40 V).

4-7. Monolayers without Annealing Treatment

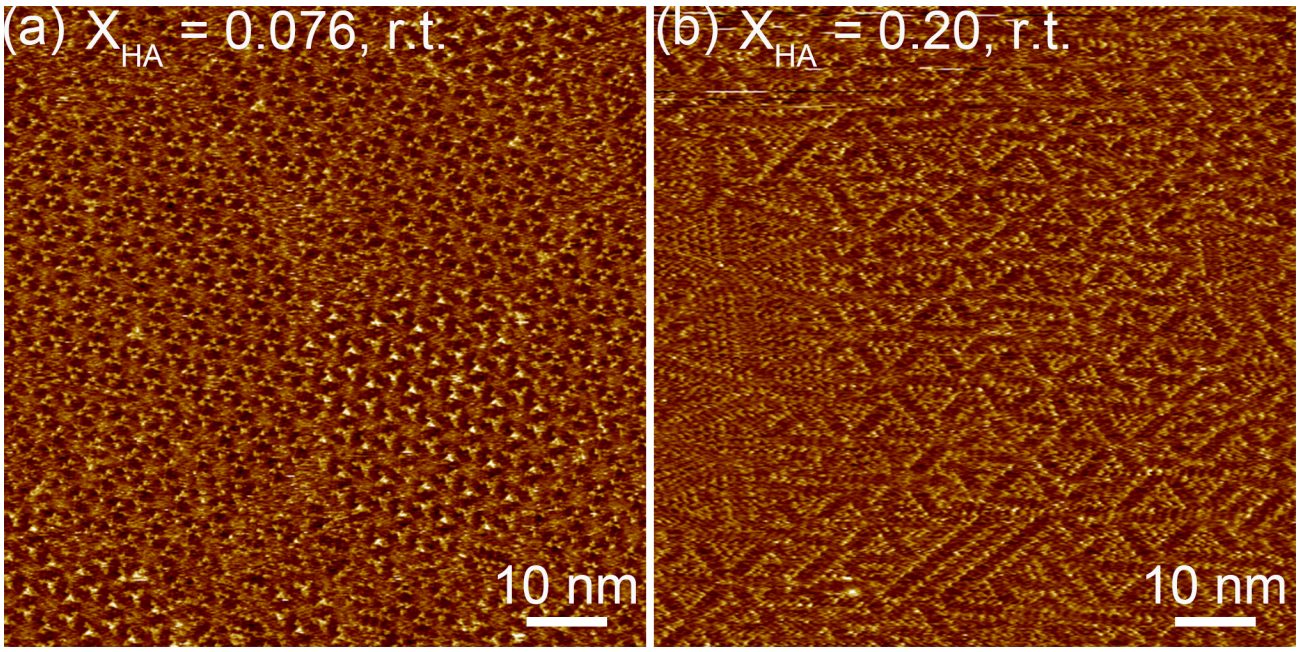

Fig. S24. STM images of SAMNs at the TCB-HA/graphite interface without annealing treatment. (a) Hexagonal porous structure and triangular cluster (n = 2) at X_{HA} = 0.076 (I_{set} = 250 pA, V_{bias} = –0.40 V). (b) Non-uniform structure at X_{HA} = 0.20 (I_{set} = 250 pA, V_{bias} = –1.20 V).

5. Triangular Cluster Formation

The DBA molecule only forms the triangular clusters rather than other clusters having different regular shapes. As the DBA molecule is a trigonal molecular building block, in addition to the observed triangular cluster, two virtual hexagonal clusters are roughly modeled (Fig. S25). For the triangular cluster (Fig. S25a), the intermolecular cyclic hydrogen bonding interactions between the hydroxy groups of DBA inside of the cluster are ideal. Moreover, at the edges, intermolecular interactions, *i.e.* hydrogen bonding interactions between the hydroxy groups of DBA and between the hydroxy group of DBA and carboxy group of HA molecule, and also van der Waals interactions between the alkoxy chains of DBAs and the solvent HA molecules are ideal. In the hexagonal cluster consisting of the seven DBA molecules having same orientations (Fig. S25b), the central molecule (m = 0) forms ideal hydrogen bonding interactions with neighboring molecules. However, although at the three edges the intermolecular interactions are ideal similar to the triangular cluster, at the remaining three edges indicated by green arrows, the DBA molecules cannot interact with each other. For another hexagonal cluster consisting of the six DBAs molecules with two different orientations (Fig. S25c), formation of favorable intermolecular hydrogen bonding interactions is not possible. These models suggest that the triangular cluster is more stable over the hexagonal clusters due to the favorable intermolecular interactions.

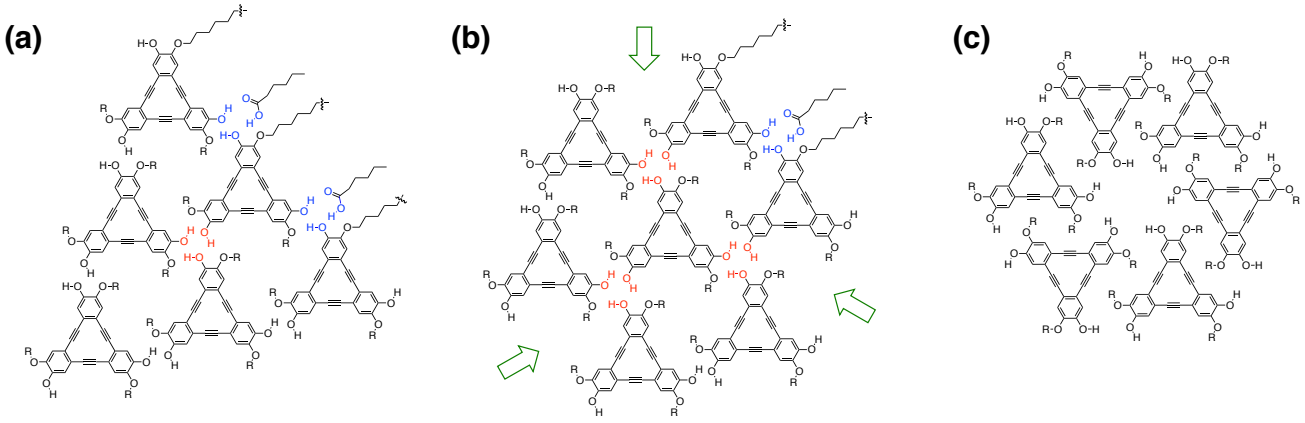

Fig. S25. Three possible cluster models, (a) triangular, (b) hexagonal-1 and (c) hexagonal-2 models. In the model, hydrogen bonding interactions between three hydroxy groups inside of the clusters are colored in red. The hydrogen bonding interactions between DBA and HA molecules are colored in blue. There are no hydrogen bonding interactions at the three edges pointed by green arrows.

6. Estimation of Solvation Energies by MM/MD Simulations

MD simulations were run in the canonical (NVT) ensemble at 298 K using the Nose-Hoover thermostat with the integration time step of 1 fs. The solvation energies of **DBA-OC14-OH** in HA and TCB were calculated by MD simulations using solvation free energy tools of the Forcite module. Three dimensional solvent boxes with periodic boundary conditions (a = 40 Å, b = 40 Å, c = 50 Å and α = β = γ = 90° for HA and a = 45 Å, b = 45 Å, c = 41 Å and α = β = γ = 90° for TCB) include 400 HA or TCB molecules. The different box sizes are set to reproduce the experimentally derived densities of TCB (1.46 g/cm³) and HA (0.93 g/cm³).[14,15] First, the pure solvent phases were equilibrated by MD simulations. Second, one DBA molecule was added to these solvent structures. The addition of **DBA-OC14-OH** causes the density increase. Therefore, four or six solvent molecules were removed. Then, the systems are equilibrated again by MD simulations. The criterion for the equilibration is that the potential energy change reaches less than 5 kcal/mol in 1 ns. For the equilibrated structures, the solvation energies were determined.

Table S1. Summary of MD Simulations.

solvent	number of solvent molecules	density (g/cm^3)	E_{vacuum}[a] (kcal/mol)	$E_{van\ der\ Waals}$[b] (kcal/mol)	$E_{electrostatic}$[c] (kcal/mol)	E_{solv}[d] (kcal/mol)
TCB	396	1.473	–3.53	–48.58	2.62	–49.49
	394	1.465	–3.76	–51.47	1.01	–54.22
HA	396	0.933	–3.65	5.154	–1.77	–0.26
	394	0.924	–3.38	5.11	–0.29	1.44

[a] Energy of the solute DBA molecule in vacuum. The molecular configuration is identical to that in solvated structure. [b] Van der Waals contribution in the solvate structure. [c] Electrostatic contribution in the solvate structure. [d] The total solvation free energy. This was calculated by the following equation; $E_{solv} = E_{vacuum} + E_{van\ der\ Waals} + E_{electrostatic}$.

7. References

1. W. Mamdouh, H. Uji-I, J. S Ladislaw, A. E. Dulcey, V. Percec, F. C. D. Schryver and S. D. Feyter, *J. Am. Chem. Soc.* **2006**, *128*, 317–325.

2. P. N. Dickerson, A. M. Hibberd, N. Oncel and S. L. Bernasek, *Langmuir* **2010**, *26*, 18155–18161.

3. L. Y. Liao, Y. B. Li, J. Xu, Y. F. Geng, J. Y. Zhang, J. L. Xie, Q. D. Zeng and C. Wang, *J. Phys. Chem. C* **2014**, *118*, 28625–28630.

4. K. Tahara, R. Nakayama, M. Maeda, S. D. Feyter and Y. Tobe, *J. Phys. Chem. C* **2019**, *123*, 27020–27029.

5. Y. Yang and C. Wang, *Chem. Soc. Rev*. **2009**, *38*, 2576–2589.

6. S. S. Jester, E. Sigmund, L. M. Röck and S. Höger, *Angew. Chem., Int. Ed*. **2012**, *51*, 8555–8559.

7. B. Ilan, G. M. Florio, M. S. Hybertsen, B. J. Berne and G. W. Flynn, *Nano Lett.* **2008**, *8*, 3160–3165.

8. T. Yang, S. Berber, J. F. Liu, G. P. Miller and D. Tománek, *J. Chem. Phys*. **2008**, *128*, 124709.

9. K. Tahara, S. Furukawa, H. Uji-I, T. Uchino, T. Ichikawa, J. Zhang, W. Mamdouh, M. Sonoda, F. C. D. Schryver, S. D. Feyter and Y. Tobe, *J. Am. Chem. Soc*. **2006**, *128*, 16613–16625.

10. F. Jäckel, M. Ai, J. Wu, K. Müllen and J. P. Rabe, *J. Am. Chem. Soc*. **2005**, *127*, 14580–14581.

11. E. Ghijsens, O. Ivasenko, K. Tahara, H. Yamaga, S. Itano, T. Balandina, Y. Tobe and S. D. Feyter, *ACS Nano* **2013**, *7*, 8031–8042.

12. K. H. Ernst, *Phys. Status Solidi B* **2012**, *249*, 2057–2088.

13. R. Raval, *Chem. Soc. Rev*. **2009**, *38*, 707–721.

14. P. Góralski and H. Piekarski, *J. Chem. Eng. Data* **2007**, *52*, 655–659.

15. J. A. Riddick, W. B. Bunger and T. K. Sakano, Wiley-Interscience: New York, 1986.